IEEE Photonics Journal
An IEEE Photonics Society Publication

Cavity Length Scaling of Quantum Cascade Lasers for Single-Mode Emission and Low Heat Dissipation, Room Temperature, Continuous Wave Operation

Volume 3, Number 1, February 2011

Richard A. Cendejas
Zhijun Liu
Wendy Sánchez-Vaynshteyn
Catherine G. Caneau
Chung-en Zah
Claire Gmachl

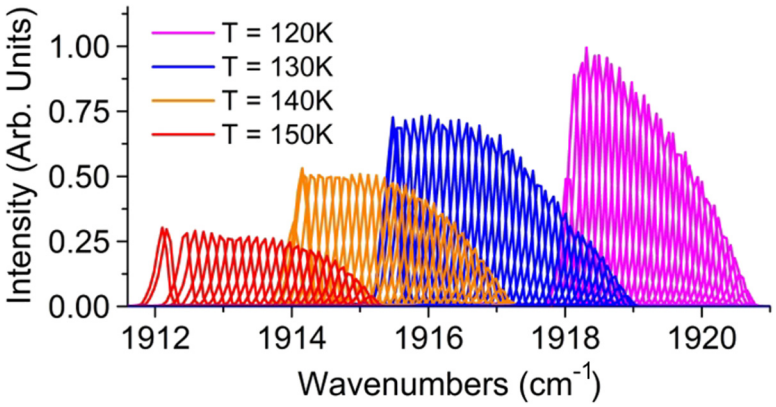

DOI: 10.1109/JPHOT.2010.2103376
1943-0655/$26.00 ©2011 IEEE

Cavity Length Scaling of Quantum Cascade Lasers for Single-Mode Emission and Low Heat Dissipation, Room Temperature, Continuous Wave Operation

Richard A. Cendejas,[1] Zhijun Liu,[1,2] Wendy Sánchez-Vaynshteyn,[1] Catherine G. Caneau,[3] Chung-en Zah,[3] and Claire Gmachl[1]

[1]Department of Electrical Engineering, Princeton University, Princeton, NJ 08540 USA
[2]Division of Engineering, Brown University, Providence, RI 02912 USA
[3]Corning Incorporated, Corning, NY 14831 USA

DOI: 10.1109/JPHOT.2010.2103376
1943-0655/$26.00 ©2011 IEEE

Manuscript received December 20, 2010; accepted December 23, 2010. Date of publication December 31, 2010; date of current version January 24, 2011. This work was supported by MIRTHE (NSF-ERC) under Grant EEC-0540832. Corresponding author: R. A. Cendejas (e-mail: rcendeja@princeton.edu).

Abstract: Single-mode operation of Fabry–Perot quantum cascade (QC) lasers is achieved through the systematic shortening of the cavity length from 764 to 110 μm. The increased mirror loss is mitigated using highly reflective (HR) metallic facet coatings ($R > 95\%$). Ultrashort cavity QC lasers operate single mode with the best device having a mode-hop free current tuning range of 3.44 cm^{-1}. Using combined heat-sink temperature and current tuning, the largest single-mode tuning range attained was 8.56 cm^{-1}. The heat dissipation of a 110-μm ultrashort cavity QC laser is 0.23 W at 80 K and 0.43 W at 150 K. With a 500-μm cavity and both facets HR coated with reflectivities of $\sim$95% and 75%, room-temperature continuous wave operation is realized with heat dissipation of 1.2–1.7 W.

Index Terms: Optical resonators, single-mode operation, quantum cascade lasers.

1. Introduction

Quantum cascade (QC) lasers have been maturing into highly power efficient, room-temperature light sources [1]–[4]. With a large design space that covers important absorption peaks of many gas species in the mid-infrared, QC lasers are rapidly becoming viable sources in portable, inexpensive systems for trace gas sensing [5], [6]. Unfortunately, the typically multi-mode emission of an as-cleaved QC laser is unsuitable for many desired applications requiring additional complexity in the QC laser or QC laser system to ensure single-mode operation. Although gain clamping of the QC laser should lead to single-mode emission in continuous wave operation, conventionally sized QC lasers, which are typically a few millimeters long, are nevertheless multi-mode, as opposed to single mode, as shown in Fig. 1(a) and (b). Grating-tuned external-cavity QC lasers can provide single-mode operation and broad tunability [7], yet they require precise optical alignment and tuning of external components, which hinders system portability and increases the system's power requirements due to the additional equipment required. Approaches such as distributed feedback (DFB) QC lasers [8]–[10], Bragg reflectors at the QC laser facets [11], and other resonator geometries [12] have each achieved single-mode operation, but they all require more complex fabrication techniques, often resulting in a lower yield.

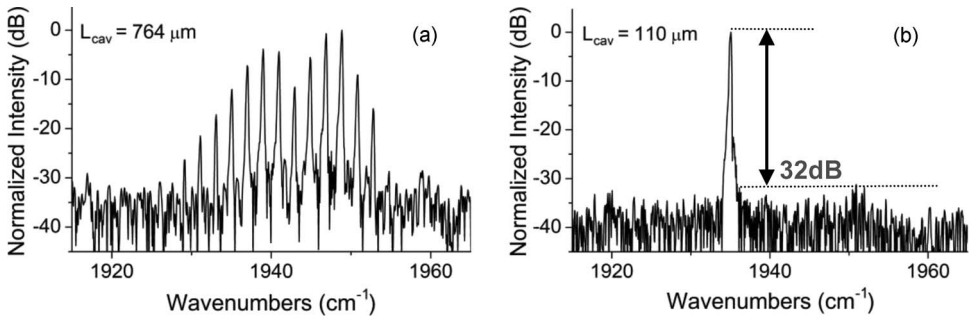

Fig. 1. (a) Multi-mode spectrum of a 764-μm-long QC laser operating at 80 K in continuous wave mode 10% above threshold current. (b) Single-mode spectrum of a 110-μm-long QC laser operating at 80 K in continuous wave mode 10% above threshold current. The side-mode suppression ratio is over 30 dB and limited by the Fourier Transform Infrared Spectrometer (FTIR) noise floor.

It is understood from laser physics principles that shortening the cavity length will increase the free spectral range (FSR), effectively pushing the side modes away from the mode closest to the gain peak, yet there is little published work on the effects of ultrashort cavities on QC laser modal behavior. While single-mode operation was obtained using 98 μm to 105 μm ultrashort cavity QC lasers with integrated deep-etched Bragg reflectors, the Bragg reflectors themselves introduce wavelength dependent effects on the microlasers [11], making it difficult to determine the effect of just the cavity length. With the added fabrication required to etch Bragg reflectors this approach is also not as manufacturable. We demonstrate here that simply cleaving ultrashort cavity QC lasers provides a more direct and cost-effective procedure that can be performed post-fabrication. Recently, [13] reported obtaining a 19-dB side-mode suppression ratio (SMSR) single-mode emission at 85 K with a 150-μm-long Fabry–Perot QC microlaser in pulsed operation by cleaving but did not achieve continuous wave operation, which is desired for trace gas sensing. Although there is an expected reduction in optical power by employing ultrashort cavity QC lasers for single-mode operation, 1–5 mW is sufficient for many spectroscopic applications [7], [14].

In the first part of this paper, we present work on the systematic reduction of the cavity length by cleaving ultrashort cavity QC lasers from 764 μm to 110 μm in order to achieve a SMSR greater than 30 dB at single-mode operation. The high mirror loss associated with as-cleaved ultrashort cavities is mitigated with evaporated metallic facet coatings to reduce the threshold current density. The best device with a cavity length of 110 μm exhibited a mode-hop free current tuning range of 3.44 cm^{-1} at 130 K and an 8.56 cm^{-1} combined current and temperature tuning range in continuous wave mode. The smaller laser dimension also leads to the added benefit of significantly lower power consumption, which is well below 0.5 W at cryogenic temperatures and 2 W at room-temperature continuous wave operation. A thorough study of such low power consuming QC lasers is discussed in detail in the second part of this paper.

2. Laser Design

The $\lambda = 5.3$ μm QC lasers in this study were designed as "two-phonon resonance" QC lasers [15]. Their electron energy band diagram is shown in Fig. 2. The layer sequence, in angstroms, of one period of active region and injector in the direction of electron flow is **40**/15/**11**/49/**12**/46/**13**/41/**24**/34/**18**/30/**19**/26/**19**/<u>26</u>/**20**/<u>25</u>/**23**/25/**23**/23/**24**/23, where the $In_{0.354}Al_{0.646}As$ barrier layers are represented in bold, $In_{0.661}Ga_{0.339}As$ well layers are shown in normal text, and the n-doped layers are underlined. The laser transition, with energy of 250 meV, is indicated by the vertical arrow in Fig. 2. The upper and lower laser level lifetimes are 1.75 ps and 0.22 ps, respectively. The optical dipole matrix element is 1.73 nm. A large energy separation of 147 meV between the lower laser level and the ground state of the next downstream injector is chosen to suppress thermal backfilling. Additionally, the energy separation between the upper laser level and the conduction band continuum is designed as 408 meV to avoid thermionic emission at high temperatures [16].

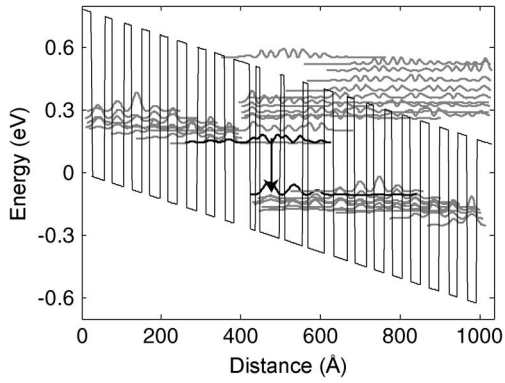

Fig. 2. Conduction band diagram of one active region sandwiched between two injectors and the moduli squared of the relevant wave functions of a $\lambda = 5.3$ μm QC laser with a 4 quantum well active region. An electric field of 63 kV/cm is applied. The bold lines represent the upper and lower lasing states, and the vertical arrow indicates the laser transition.

Optimization of the waveguide and active region doping concentration will be discussed further in Section 4, where three different wafers (E1, E2, E3) varying in doping density are used.

3. Single-Mode Operation

3.1. Fabrication

The wafer used in single-mode study was the lowest doped in the active region: wafer E3. The wafer was patterned into ridge waveguide lasers that were 9 μm, 11 μm, 13 μm, and 15 μm wide. An isotropic wet etch $(HNO_3 : HBr : H_2O = 1 : 1 : 10)$ was used to form the ridges with a depth of 10 μm. An insulating layer of 3000 Å of Si_3N_4 was grown by plasma enhanced chemical vapor deposition. Contact windows on top of the ridge were exposed into the nitride to allow for electrical contacts to the laser. Thin metal contacts of 250 Å titanium and 1500 Å gold were deposited using an e-beam evaporator. The substrate was thinned down to 80 μm to facilitate cleaving of ultrashort cavities. A germanium and gold contact was then deposited on the bottom of the substrate. Device bars containing several lasers were cleaved and mounted epitaxial-side-up on copper blocks using Indium alloy.

Light–Current–Voltage $(L-I-V)$ measurements in pulsed and continuous wave modes were recorded to characterize the as-cleaved devices. The back-facet of the device chip was then coated with a highly reflective (HR) metallic coating consisting of a 3000-Å insulating layer of SiO_2, a 250-Å Ti adhesion layer, 1500 Å of Au, and 500 Å of SiO_2. The back-facet reflectivity was determined to be greater than 95% by evaluating the change in lasing threshold from uncoated to back-facet coated cavity. For ultrashort cavity QC lasers that did not lase with only a back-facet HR coating, a partially reflecting front-facet coating of SiO_2/Ti/Au/SiO_2 of thicknesses 2500/200/250/500 Å was used. These thicknesses allowed for measurable amounts of light emitted and an increase in the front-facet reflectivity from ~29% to over 75%, increasing the combined mirror reflectivity $R_1 \times R_2$ from 8.4% to over 70%. Ideally, low-loss dielectric facet coatings would have been used instead, as metallic coatings absorb the transmitted laser light, but the required materials and equipment were not available to us at the time.

3.2. Model

Cavity length scaling utilizes an inherent laser property where the separation between the allowed resonator modes, or free spectral range (FSR), increases as the cavity length decreases given by the equation $\nu_{FSR} = (2\, n_{eff} L_{cav})^{-1}$, where n_{eff} is the effective modal index, and L_{cav} is the cavity length of the QC laser. The gain at each resonator mode is given by the envelope of the gain

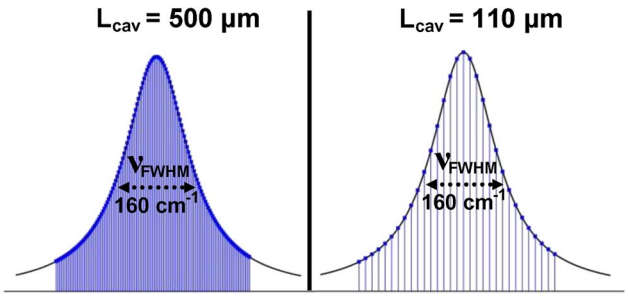

Fig. 3. Pictorial representation of the resonator modes in a laser together, represented by the position of the vertical lines and blue dots, with a Lorentzian gain curve. The free spectral range (FSR) increases with decreasing cavity length from 3 cm^{-1} to 13 cm^{-1} when the cavity length decreases from 500 μm to 110 μm.

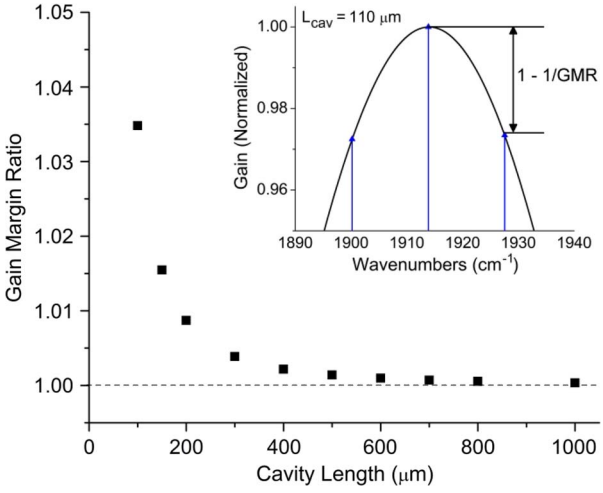

Fig. 4. Maximum gain margin ratio of the lasing mode over the adjacent side mode with respect to cavity length. As the cavity length decreases below 500 μm to 100 μm, the gain margin ratio increases from 1.0014 to 1.035, as the side modes move further away from the gain peak. Inset: Closeup of the resonator modes and gain curve near the gain peak for $L_{cav} = 110$ μm. The ideal case of the lasing mode overlapping with the gain peak and the experimentally determined gain curve modeled using a Lorentzian line shape with FWHM of 160 cm^{-1} is used to determine a gain margin ratio for various cavity lengths.

curve at the resonator mode frequency. The typical gain curve of QC lasers is Lorentzian with a full-width at half-maximum (FWHM) of about 10% of the lasing wavelength. From electroluminescence measurements taken from deep-etched semicircular mesas at operating conditions similar to those of the QC lasers measured, the FWHM of the $\lambda = 5.3$ μm QC lasers is $\sim$160 cm^{-1}. A pictorial representation of the allowed resonator modes for an $L_{cav} = 500$ μm and 110 μm bounded by the experimentally determined Lorentzian gain curve is in Fig. 3.

The gain margin ratio between the peak modal gain and the nearest adjacent side mode gain ratio increases from 1.0014 at $L_{cav} = 500$ μm to 1.035 at $L_{cav} = 110$ μm, as shown in Fig. 4. The ideal case where one resonator mode overlaps the gain peak and the adjacent side modes lie symmetrically along the gain curve is used to determine the resonator mode gain values, as shown in the inset of Fig. 4. For cavity lengths above 500 μm, the gain margin ratio is less than 1.001, i.e., neighboring modes near the gain peak experience practically the same gain; yet at cavity lengths smaller than 200 μm, the side modes move further down the gain curve, and the gain margin ratio increases rapidly. With a higher gain margin ratio, we expect single-mode operation as the gain for the lasing mode becomes noticeably greater than for the adjacent side modes.

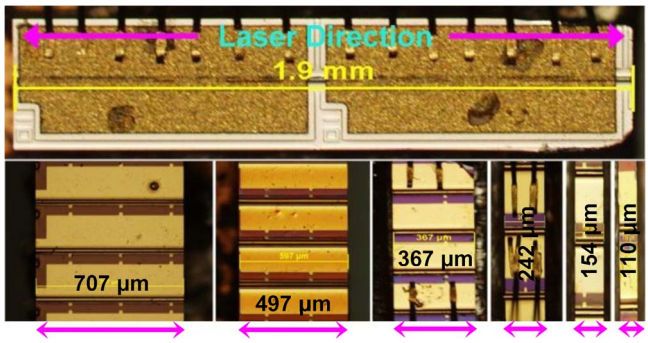

Fig. 5. Ultrashort cavity QC lasers selected within our L_{cav} range of 764 μm to 110 μm (bottom) and a more typically sized 1.9-mm QC laser (top) for comparison. Conventionally sized QC lasers range from 2 mm to 4 mm.

3.3. Device Results

A device was deemed single mode only when the SMSR exceeded 30 dB, as shown in Fig. 1(b). The ultrashort cavity QC lasers were operated both in pulsed and continuous wave; however, under pulsed operation, all devices remained multi-mode, despite exhibiting single-mode operation in continuous wave. Thirty seven ultrashort cavity QC lasers were cleaved by hand with L_{cav} ranging from 764 μm to 110 μm and 25 devices operated continuous wave at 80 K and above. Photographs in Fig. 5 show a size comparison of the ultrashort cavity QC lasers and a conventionally sized QC laser. The packaging yield for devices shorter than 200 μm was under 25% due to cracked facets and the difficulty associated with mounting by hand. Higher yields could be obtained with specialized equipment.

The FSR $(2n_{eff}L_{cav})^{-1}$ for each device was extracted from either the lasing spectrum, or from the amplified spontaneous emission spectrum for devices that operated single mode, and is shown in Fig. 6(a). An effective mode refractive index of $n_{eff} = 3.325$ was extracted from the experimentally determined FSR fit curve. While the cavity lengths ranging from 764 μm to 242 μm showed a reduction in modes due to their increased FSR of 1.97 cm^{-1} to 6.2 cm^{-1}, respectively, the emission was still multi-mode. While the number of modes tend to decrease as the cavity length decreases, as seen in Fig. 6, for cavities longer than 200 μm, the emission was multi-mode. From Figs. 4 and 6, one can see that a large increase in FSR results in a large increase in gain margin between the lasing mode and the adjacent side modes, which ultimately leads to single-mode emission in continuous wave operation.

Three ultrashort QC lasers with sizes of 154 μm and 110 μm showed 30-dB SMSR single-mode emission beyond 10% of their threshold current. The 154-μm ultrashort QC laser operated single mode until 16% above threshold. When a QC laser operates in continuous wave mode, the increase in current results in a higher active region temperature, increasing the effective index of refraction and the cavity length. The refractive index increase can be substantial, such as from 3.26 to 3.32 for the lasers here with a current increase of 13.9 mA at a $\sim$9.0–9.6 V operating voltage. For a tuning current of 3.6 mA, the 154-μm-long device has a tuning range of 0.52 cm^{-1}at 108 K.

The best 110-μm device operated single mode to over 40% of its threshold current for a tuning current of 13.9 mA at 130 K. The single-mode current tuning range of the best device was 3.44 cm^{-1}. Employing heat-sink temperature tuning in addition to current tuning, a combined single-mode tuning range of 8.56 cm^{-1} was obtained, as shown in Figs. 7 and 8(a). These tuning ranges are comparable with those values found in literature for DFB-QC lasers [5]. The mode-map of the best device is shown in Fig. 8(a). The 110-μm QC laser resonator modes current tune at a rate of ~ -0.25 cm^{-1}/mA found from the linear component of the data fit. The electroluminescence gain curve peak, as seen in Fig. 8(b), red-shifts with heat-sink temperature at a nearly linear rate. The "back-and-forth" mode-hops seen in Fig. 8(a) can be explained by the competing tuning rates of the QC laser resonator modes and gain curve peak with current and temperature, as a different lasing mode is selected based on the gain curve overlap with the resonator modes.

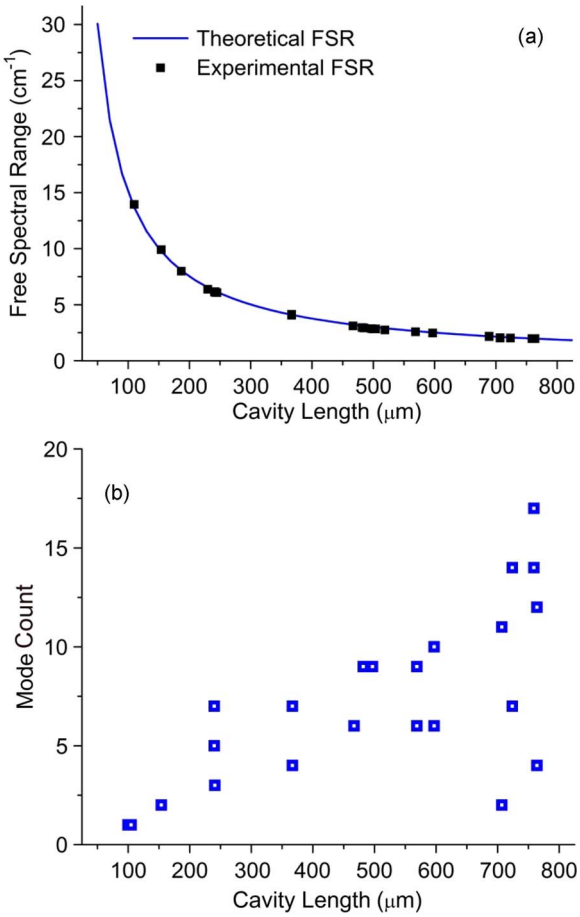

Fig. 6. (a) Experimentally determined FSR for ultrashort cavity QC lasers (square points) and experimental modal refractive index of $n = 3.325$ results from the fit to a simple FSR $(2n_{\text{eff}}L_{\text{cav}})^{-1}$ curve. (b) Range of mode counts per cavity length bin taken at 10% above threshold in continuous wave. The number of experimental mode counts decreased significantly at a cavity length of $\sim$200 μm due to a greater FSR increasing the gain margin of the side modes.

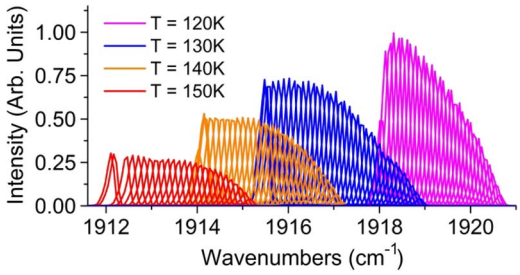

Fig. 7. Mode-hop free tuning of a 110-μm ultrashort cavity QC laser operating continuous wave. At heat-sink temperatures of 120 K, 130 K, 140 K, and 150 K, the mode-hop free current tuning range was 2.65 cm^{-1}, 3.44 cm^{-1}, 3.02 cm^{-1}, and 3.08 cm^{-1}, respectively. The combined mode-hop free tuning range is 8.56 cm^{-1}.

As a result, wavelength tuning can be performed using a combination of heat-sink temperature and current tuning. Higher absolute heat-sink temperatures could be obtained with better thermal management such as epitaxial-side-down mounting and thick gold electroplating [16], [17]. With these strategies, ultrashort cavity QC lasers could serve as single-mode sources for room-temperature applications requiring low input power and ease of integration.

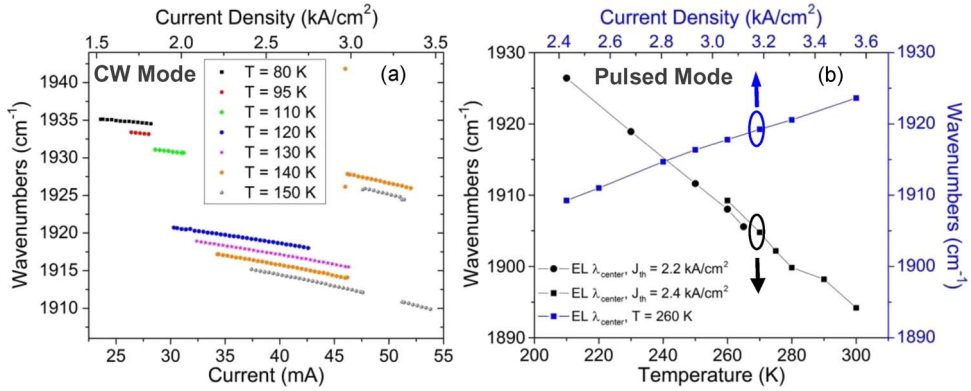

Fig. 8. (a) Mode map of the best device with cavity length of 110 μm at various heat-sink temperatures operated in continuous wave mode. Mode-hops are a result of different gain curve peak and resonator modes tuning rates. (b) The temperature and current tuning rate of a deep-etched mesa in pulsed operation is about -0.37 cm^{-1}/K and 12 cm^{-1}/(kA/cm^2).

4. Power Consumption and Heat Dissipation

An added benefit of ultrashort cavity QC lasers is that their power consumption is low: 0.23 W to 0.43 W for the 110-μm-long ultrashort cavity QC laser measured. Power consumption scales with laser dimension and scaling the laser dimension is a post-fabrication technique that can be used to reduce the power requirements and heat dissipation of a QC laser from the conventional 5–10 W to a more manageable 1–2 W. In the following sections, we discuss the optimization of short-cavity lasers for low power consumption operation.

4.1. Doping Optimization and Laser Fabrication

The design of the active regions and injectors of the lasers have already been discussed in Section 2. Although active region doping optimization of QC lasers has been carried out in other published work [18]–[20], here, we focus on the waveguides and include both active region doping and waveguide doping optimizations for completeness. In order to overcome the uncertainty in background doping, three waveguides with modified doping levels are implemented with the same active core design. For the first wafer E1, the doping for the four injector layers is at a concentration of 1.8×10^{17} cm^{-3}. Twenty-six periods of active regions and injectors are sandwiched between 0.2-μm-thick low doped $(5 \times 10^{16}$ cm$^{-3})$ $In_{0.53}Ga_{0.47}As$ layers. The bottom cladding is a low doped InP buffer layer $(1 \times 10^{17}$ cm$^{-3})$. The top waveguide claddings consist of a 2.5-μm-thick low doped $(1 \times 10^{17}$ cm$^{-3})$ InP, followed by a 1.2-μm-thick highly doped $(8 \times 10^{18}$ cm$^{-3})$ InP plasmon layer and a heavily doped $(1 \times 10^{19}$ cm$^{-3})$ 0.01-μm-InP contact layer. For the second wafer E2, the doping levels in the InP top and bottom waveguide claddings were reduced by half from 1×10^{17} to a reduced doping of 0.5×10^{17} cm^{-3} with the doping levels in other layers the same as E1. For the third wafer E3, the doping levels in both InP waveguide cladding layers and the active core were reduced by half, as compared with E1 as the doping levels in upper and lower InP waveguide claddings are decreased from 1×10^{17} to 0.5×10^{17} cm^{-3}, and the doping level in the active core is reduced from 1.8×10^{17} to 0.9×10^{17} cm^{-3}.

These three wafers were grown by metal-organic chemical vapor deposition (MOCVD). The wafers were processed into deep-etched, narrow ridge waveguide lasers with a $\sim$7-μm-thick electroplated gold top contact. The processing steps are described in [21]. The QC lasers were cleaved into conventional 3.5-mm-long cavities with back-facet high reflectivity coatings of SiO_2/Ti/Au/SiO_2 and thicknesses of 3500/150/1500/1000 Å. In order to reduce the heat dissipation, much shorter 0.5-mm-long lasers were also cleaved, and their back and front facets were HR coated with SiO_2/Ti/Au/SiO_2 of thicknesses 3500/150/1500/1000 Å and 3500/150/110/1000 Å, respectively. All these lasers were epitaxial-side-up mounted on copper blocks for testing. Fig. 9 shows a representative 0.5-mm-long QC laser and a conventional 3.5-mm-long QC laser for comparison.

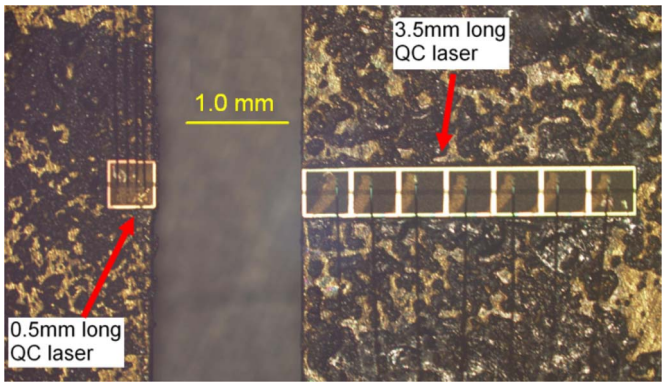

Fig. 9. Optical image of a 0.5-mm-long, epitaxial-side-up mounted QC laser (left). For comparison, a conventional 3.5-mm-long, epitaxial-side-up mounted QC laser is also shown (right).

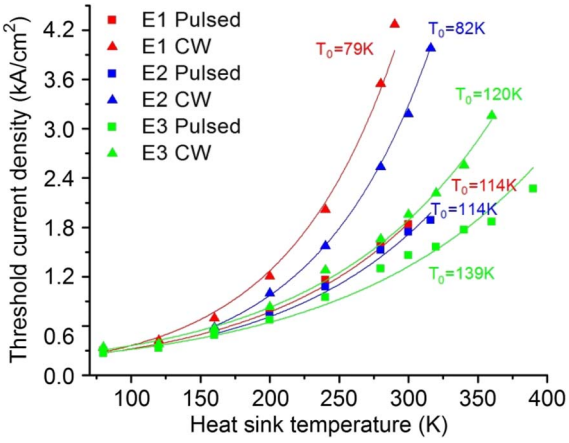

Fig. 10. Threshold current density versus heat-sink temperature in both pulsed and continuous wave operation for three QC laser wafers: E1, E2, and E3, with different doping levels. The red data points are the thresholds for a back-facet HR coated, 3.5-mm-long, 9.7-μm-wide QC laser from E1; the blue data points are the thresholds for a back-facet HR coated, 3.5-mm-long, 8.4-μm-wide QC laser from E2; the green data points are the thresholds for a back-facet HR coated, 3.5-mm-long, 7.6-μm-wide QC laser from E3. The lines are exponential fits.

4.2. Device Results

Fig. 10 shows the measured threshold current densities versus heat-sink temperature of 3.5-mm-long QC lasers from the three wafers with different doping levels in both pulsed and continuous wave operation. For the highest doped wafer E1, as the temperature increases from 80 to 300 K, the pulsed laser threshold current density increased from 0.30 to 1.84 kA/cm^2. In continuous wave operation, the threshold current density increased from 0.33 kA/cm^2 at 80 K to 4.27 kA/cm^2 at the maximum operating temperature of 290 K. For E2, with the doping reduced by half in the waveguide claddings, the pulsed threshold current was $\sim$5% lower than that of E1, and the maximum continuous wave temperature increased to 316 K. For the lowest doped wafer E3, with the doping level in the active core reduced by half, the pulsed threshold current density was lowered by $\sim$16% as compared with E2, and the maximum continuous wave temperature increased to 360 K. From the exponential fit curves, the characteristic temperature T_0 for E1 is extracted as 114 K and 79 K in pulsed and continuous wave operation, respectively. E2 has a T_0 similar to that of E1, which is expected since no change was made to the doping level in the active core for these two wafers. With less doping in the active core, E3's T_0 increased to 139 K and 120 K in pulsed and continuous wave operation, respectively. This increase in T_0 is due to the suppression of doping-related thermal effects such as thermal backfilling [22] or intersubband absorptions [23].

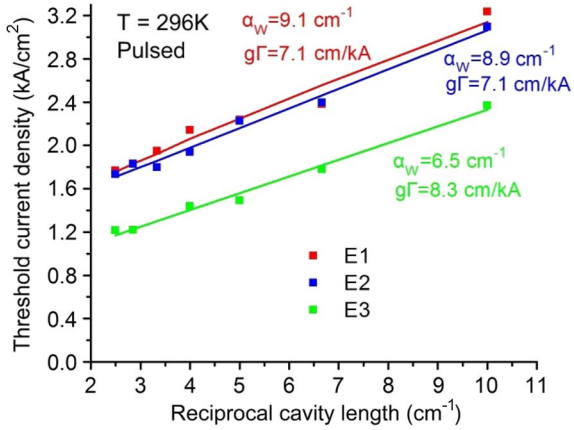

Fig. 11. Pulsed threshold current density versus reciprocal cavity length at 296 K for QC lasers from wafers E1, E2, and E3. The lines are the results of linear least squares fits.

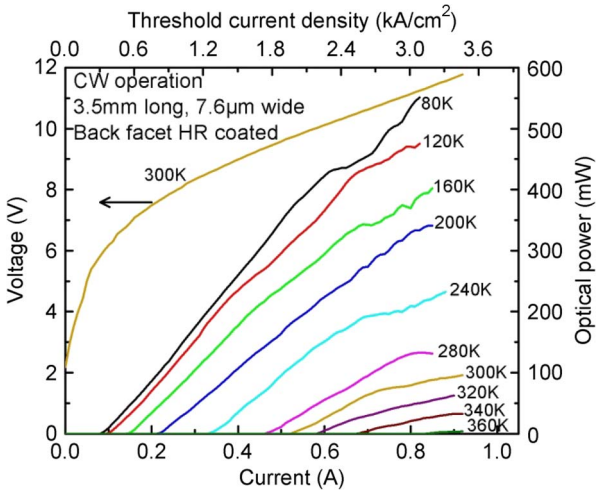

Fig. 12. Continuous wave $L-I$ curves of a back-facet HR coated, 3.5-mm-long, 7.6-μm-wide QC laser at various heat-sink temperatures. The $I-V$ curve at 300 K is also given.

To explicitly examine the effects of the doping levels, we measured the optical gain coefficient and waveguide loss of these three wafers using the "$1/L$" method at room temperature, as shown in Fig. 11. The extracted gain coefficient and waveguide loss for E1 are 7.1 cm/kA and 9.1 cm^{-1}, respectively. E2, with reduced doping level in the waveguide cladding, has the same gain coefficient and a similar waveguide loss of 8.9 cm^{-1}. E3, with reduced doping levels in both the waveguide cladding layer and active core, has a gain coefficient of 8.3 cm/kA, which is greater than the two higher doped wafers E1 and E2. Its extracted waveguide loss is 6.5 cm^{-1}, which is smaller by 2.6 cm^{-1} than that for E1 owing to the lower doping. From these comparisons, we can see that the doping in the active core is a more important factor than that of the waveguide cladding in reducing the waveguide loss and significantly increasing the laser performance.

Fig. 12 shows the continuous wave $L-I$ curves of a conventionally sized, 3.5-mm-long, 7.6-μm-wide, back-facet HR coated QC laser from the lowest threshold wafer E3 at various heat-sink temperatures. It emitted more than 550 mW at 80 K and operated up to 360 K. At room temperature, it emitted an optical power of $\sim$100 mW with a threshold current density of 1.95 kA/cm^2. The heat dissipation for room-temperature continuous wave operation is 5–11 W, which is a large thermal load similar to previously reported high-performance QC lasers [21].

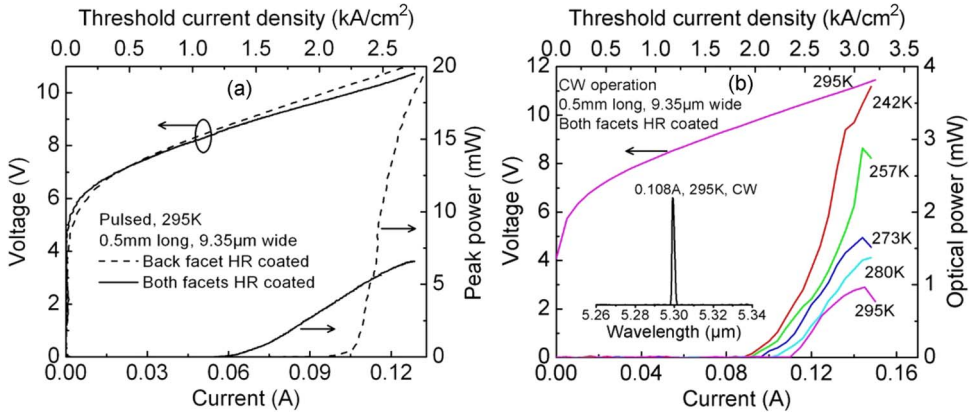

Fig. 13. (a) Pulsed $L-I-V$ curves for a 0.5-mm-long, 9.35-μm-wide QC laser from wafer E3 with back-facet (dashed line) and both facets (solid line) HR coated at 295 K. (b) Continuous wave $L-I$ curves of the laser with both facets HR coated at various heat-sink temperatures. The $I-V$ curve at 295 K is also given. The inset shows the laser spectrum at 295 K and 0.108 A.

In order to reduce the large heat dissipation, much shorter 0.5-mm-long QC lasers were tested. Fig. 13(a) shows the pulsed $L-I-V$ curves at room temperature for a 0.5-mm-long laser with one facet and both facets HR coated. The as-cleaved 0.5-mm-long laser did not lase due to the large mirror loss. After adding the HR coating on the back-facet, it lased with a threshold current density of 2.24 kA/cm^2. After adding the HR coating on the front facet, the laser threshold decreased to 1.16 kA/cm^2. With this threshold change, the gain coefficient and waveguide loss given in Fig. 11, the reflectivity is estimated as $\sim$95% and 75% for the HR coating on the back and front facets, respectively. Fig. 13(b) shows the $L-I$ curves of the laser with both facets HR coated operated in continuous wave. It emitted a maximum power of $\sim$1 mW at 295 K with a threshold current density of 2.35 kA/cm^2. Its heat dissipation is reduced to 1.13–1.64 W, which is $\sim$5 times smaller than that of the conventionally sized QC laser shown in Fig. 12. As a few milliwatts of optical power is satisfactory for most of the trace-gas sensing applications based on optical point detection schemes, this HR coated short cavity QC laser represents an effective approach in reducing the heat dissipation. With further optimization to lower the laser threshold, better laser layout, and packaging, such as buried heterostructure fabrication with a narrow laser ridge and epitaxial-side-down mounting, further reduction in heat dissipation and operating power is possible.

5. Summary

Single-mode operation of Fabry–Perot QC lasers is achieved through the systematic shortening of the cavity length from 764 μm to 110 μm. The increased mirror loss is mitigated using HR metallic facet coatings. Scaling of the cavity length to 154 μm and 110 μm achieved 30-dB SMSR single-mode operation up to 16% and over 40% above laser threshold, respectively. For the best 110-μm device, the mode-hop free tuning range of 3.44 cm^{-1} was achieved at 130 K with a current tuning of 13.9 mA, and the combined heat-sink temperature and current tuning range gave a total tuning range of 8.56 cm^{-1}. The heat dissipation of the best 110-μm ultrashort cavity QC laser is 0.23 W at 80 K and 0.43 W at 150 K. Scaling the cavity length down to 0.5 mm and with both facets HR coated with reflectivities of $\sim$95% and 75% to compensate for the greater mirror loss, room-temperature continuous wave operation is realized with heat dissipation of 1.2–1.7 W, in contrast to 5–11 W for a conventionally sized QC laser. Dielectric front-facet coatings and better thermal management such as epi-side down mountings are industry-standard fabrication techniques that could simultaneously demonstrate both single-mode operation and continuous-wave, room-temperature operation. Cavity length scaling represents a straightforward approach to single-mode emission with the additional advantage of facilitating the cooling of high-performance QC lasers and the development of compact, portable sensor systems.

Acknowledgment

The authors appreciate the discussions with D. Qu during the early part of this work.

References

[1] P. Liu, A. Hoffman, M. Escarra, K. Franz, J. Khurgin, Y. Dikmelik, X. Wang, J. Fan, and C. Gmachl, "Highly power-efficient quantum cascade lasers," *Nat. Photon.*, vol. 4, no. 2, pp. 95–98, Feb. 2010.
[2] Y. Bai, S. Slivken, S. Kuboya, S. Darvish, and M. Razeghi, "Quantum cascade lasers that emit more light than heat," *Nat. Photon.*, vol. 4, no. 2, pp. 99–102, Feb. 2010.
[3] M. Razeghi, S. Slivken, Y. Bai, B. Gokden, and S. Darvish, "High power quantum cascade lasers," *New J. Phys.*, vol. 11, p. 125017, Dec. 2009.
[4] A. Lyakh, R. Maulini, A. Tsekoun, R. Go, C. Pflügl, L. Diehl, Q. Wang, F. Capasso, and K. Patel, "3 W continuous-wave room temperature single-facet emission from quantum cascade lasers based on nonresonant extraction design approach," *Appl. Phys. Lett.*, vol. 95, no. 14, p. 141113, Oct. 2009.
[5] A. Kosterev, G. Wysocki, Y. Bakhirkin, S. So, R. Lewicki, M. Fraser, F. Tittel, and R. Curl, "Applications of quantum cascade lasers to trace gas analysis," *Appl. Phys. B*, vol. 90, no. 2, pp. 165–176, 2008.
[6] C. Bauer, A. Sharma, U. Willer, J. Burgmeier, B. Braunschweig, W. Schade, L. Hvozdara, A. Müller, and G. Holl, "Potentials and limits of mid-infrared laser spectroscopy for the detection of explosives," *Appl. Phys. B*, vol. 92, no. 3, pp. 327–333, 2008.
[7] M. Phillips and N. Ho, "Infrared hyperspectral imaging using a broadly tunable external cavity quantum cascade laser and microbolometer focal plane array," *Opt. Express*, vol. 16, no. 3, pp. 1836–1845, Feb. 2008.
[8] A. Wittmann, Y. Bonetti, M. Fischer, J. Faist, S. Blaser, and E. Gini, "Distributed-feedback quantum cascade lasers at 9 μm operating in continuous wave up to 423 K," *IEEE Photon. Technol. Lett.*, vol. 21, no. 12, pp. 814–816, Jun. 2009.
[9] S. Blaser, A. Baechle, S. Jochum, L. Hvozdara, G. Vandeputte, S. Brunner, S. Hansmann, A. Muller, and J. Faist, "Low-consumption (below 2 W) continuous-wave single mode quantum-cascade lasers grown by metal-organic vapour-phase epitaxy," *Electron. Lett.*, vol. 43, no. 22, pp. 1201–1202, Oct. 2007.
[10] F. Xie, C. Caneau, H. LeBlanc, N. Visovsky, S. Coleman, L. Hughes, and C. Zah, "High-temperature continuous-wave operation of low power consumption single-mode distributed-feedback quantum-cascade lasers at $\lambda \approx 5.2$ μm," *Appl. Phys. Lett.*, vol. 95, no. 9, p. 091110, Aug. 2009.
[11] S. Höfling, J. Reithmaier, and A. Forschel, "Device performance and wavelength tuning behavior of ultra-short quantum-cascade microlasers with deeply-etched Bragg-mirrors," *IEEE J. Sel. Topics Quantum Electron.*, vol. 11, no. 5, pp. 1048–1054, Sep./Oct. 2005.
[12] Y. Wakayama, S. Iwamoto, and Y. Arakawa, "Switching operation of lasing wavelength in mid-infrared ridge-waveguide quantum cascade lasers coupled with microcylindrical cavity," *Appl. Phys. Lett.*, vol. 96, no. 17, p. 171104, Apr. 2010.
[13] Y. Gao, J. Liu, F. Liu, W. Zhang, Q. Zhang, W. Liu, L. Liu, L. Wang, and Z. Wang, "Single-mode GaAs/AlGaAs quantum cascade microlasers," *J. Semicond.*, vol. 30, no. 11, p. 114007, Nov. 2009.
[14] Y. Bakharkin, A. Kosterev, R. Curl, F. Tittel, D. Yarekha, L. Hvozdara, M. Giovannini, and J. Faist, "Sub-ppbv nitric oxide concentration measurements using cw thermoelectrically cooled quantum cascade laser-based integrated cavity output spectroscopy," *Appl. Phys. B*, vol. 82, no. 1, pp. 149–154, 2006.
[15] J. Faist, D. Hofstetter, M. Beck, T. Aellen, M. Rochat, and S. Blaser, "Bound-to-continuum and two-phonon resonance quantum-cascade lasers for high duty cycle, high-temperature operation," *IEEE J. Quantum Electron.*, vol. 38, no. 6, pp. 533–546, Jun. 2002.
[16] A. Hamadou, J. Thobel, and S. Lamari, "Modeling of temperature effects on the characteristics of mid-infrared quantum cascade lasers," *Opt. Commun.*, vol. 281, no. 21, pp. 5385–5388, Nov. 2008.
[17] V. Spagnolo, A. Lops, G. Scamarcio, M. Vitiello, and C. Di Franco, "Improved thermal management of mid-IR quantum cascade lasers," *J. Appl. Phys.*, vol. 103, no. 4, p. 043103, Feb. 2008.
[18] T. Aellen, M. Beck, N. Hoyler, M. Giovannini, and J. Faist, "Doping in quantum cascade lasers. I. InAlAs-InGaAs/InP midinfrared devices," *J. Appl. Phys.*, vol. 100, no. 4, p. 043101, Aug. 2006.
[19] E. Mujagic, M. Austerer, S. Schartner, M. Nobile, L. Hoffmann, W. Schrenk, G. Strasser, M. Semtsiv, I. Bayrakli, M. Wienold, and W. Masselink, "Impact on doping on the performance of short-wavelength InP-based quantum-cascade lasers," *J. Appl. Phys.*, vol. 103, no. 3, p. 033104, Feb. 2008.
[20] S. Slivken and M. Razeghi, "Development of quantum cascade lasers for high peak output power and low threshold current density," *Solid State Electron.*, vol. 46, no. 10, pp. 1531–1534, Oct. 2002.
[21] Z. Liu, D. Wasserman, S. Howard, A. Hoffman, C. Gmachl, X. Wang, T. Tanbun-Ek, L. Cheng, and F. Choa, "Room-temperature continuous-wave quantum cascade lasers grown by MOCVD without lateral regrowth," *IEEE Photon. Technol. Lett.*, vol. 18, no. 12, pp. 1347–1349, Jun. 2006.
[22] J. Devenson, O. Cathabard, R. Teissier, and A. Barano, "High temperature operation of $\lambda \approx 3.3$ μm quantum cascade lasers," *Appl. Phys. Lett.*, vol. 91, no. 14, p. 141106, Oct. 2007.
[23] A. Wittmann, T. Gresch, E. Gini, L. Hvozdara, N. Hoyler, M. Giovannini, and J. Faist, "High-performance bound-to-continuum quantum-cascade lasers for broad-gain applications," *IEEE J. Quantum Electron.*, vol. 44, no. 1, pp. 36–40, Jan. 2008.